Journal of Luminescence 201 (2018) 148–155

Contents lists available at ScienceDirect

Journal of Luminescence

journal homepage: www.elsevier.com/locate/jlumin

Highly luminescent film as enhancer of photovoltaic devices

S. González-Pérez[a], J. Sanchiz[b,*], V.D. Rodríguez[c], D. Cañadillas-Ramallo[c], J. González-Platas[d], D. Borchert[e], B. González-Díaz[a], C. Hernández-Rodríguez[c], R. Guerrero-Lemus[c]

[a] Departamento de Ingeniería Industrial. Universidad de La Laguna, Avda. Astrofísico Francisco Sánchez, 38206 La Laguna, Tenerife, Spain
[b] Departamento de Química, Instituto de Materiales y Nanotecnología. Universidad de La Laguna, Avda. Astrofísico Francisco Sánchez, 38206 La Laguna, Tenerife, Spain
[c] Departamento de Física, Instituto de Materiales y Nanotecnología. Universidad de La Laguna, Avda. Astrofísico Francisco Sánchez, 38206 La Laguna, Tenerife, Spain
[d] Departamento de Física, Universidad de La Laguna, Avda. Astrofísico Fco. Sánchez, 38206 La Laguna, Tenerife, Spain
[e] Fraunhofer Institute for Solar Energy Systems, Laboratory, and Servicecenter Gelsenkirchen, Auf der Reihe 2, 45884 Gelsenkirchen, Germany

A B S T R A C T

The most extended Si based conventional photovoltaic cells show low efficiency in the UV region, however this low efficiency can be enhanced by the use of suitable down-shifters or down-converters which transform the wavelength of the incoming radiation into a wavelength for which the Si based cells have high efficiency. In this sense europium(III) luminescent benzoate and phenanthroline (and derivatives) complexes are good candidates for such purposes since they exhibit large absorption at wavelengths below 400 nm and significant emissions at the VIS range. In this work we report the synthesis the crystal structure and the spectroscopic properties of two new Eu^{3+} and Gd^{3+} complexes with the ligands 4,7-biphenyl-1,10-phenanthroline (bphen) and benzoate (bz), namely, $[Eu_2(bphen)_2(bz)_6]$ (**1**) and $[Gd_2(bphen)_2(bz)_6]$ (**2**). The X-ray single crystal study reveals a dinuclear molecular structure for the Eu^{3+} complex with two bridging benzoate ligands between the two equivalent Eu^{3+} ions. The Powder X-ray diffraction study shows that the Eu^{3+} and Gd^{3+} compounds are isostructural and allows the use of the Gd^{3+} compound for the characterization of the excited states of the complexes which were investigated to explain the sensitization process that lead to intense red emission of Eu^{3+} ions under UV excitation. The photoluminescence study of the lanthanide complexes at 15 K and 297 K revealed very efficient energy transfer processes from the antenna to the emitting Eu^{3+} ions and a high overall quantum yield. Moreover, the ligands provide rigidity, high stability and solubility to the complex in CH_2Cl_2, allowing the preparation of poly(methylmethacrylate)-doped films that can be used to cover photovoltaic devices. The analysis of external quantum yield and quantum efficiency (EQE) show its potential application to the solar cell technology with an enhancement EQE in the UV region (280–360 nm) that reaches a 4.5% at 300 nm.

1. Introduction

Photovoltaic cells and modules directly convert solar radiation into electricity, reaching more than 295 GW of cumulative installed capacity worldwide in 2016, showing a continuous increase that has doubled global production in the las three years (140 GW in 2013) [1]. Several technologies are available in this area of continuous research, but about 93% of the global PV production is based on silicon [2]. Most of these cells show low efficiencies in the UV region because of: (i) absorption and reflection losses caused by the front glass; (ii) absorption in the encapsulation material; (iii) parasitic absorptions and reflections due to the optimized λ/4 anti-reflective coatings at 600 nm; and (iv) high recombination rates in the heavily doped emitter [3]. One of the technologies that can increase the external quantum efficiency (EQE) in the UV range for standard solar cells is based on the down-conversion (DC) and down-shifting (DS) of UV photons to longer wavelength radiations in the visible range, where the EQE of solar cells is closer to 1 [4–10]. In this sense, lanthanide-organic hybrid materials have attracted great interest due to their excellent luminescent properties featuring, for instance, long decay times and sharp emission bands that have led to excellent technological applications in flat-panel displays, solid-state lighting, lasers and UV or oxygen sensors [11–13]. Nevertheless, our interest in this field arises from the ability of some of these hybrid materials to convert the UV radiation into visible light and their application in PV cells [14].

Red emission of Eu^{3+} complexes has led to many theoretical and experimental studies where the luminescent properties and the mechanism of the phenomenon have been deeply investigated [15–18]. The lanthanide ions themselves have very poor absorption properties, but this can be considerably improved by the antenna effect produced

* Corresponding author.
E-mail address: jsanchiz@ull.edu.es (J. Sanchiz).

https://doi.org/10.1016/j.jlumin.2018.04.038
Received 16 May 2017; Received in revised form 13 April 2018; Accepted 16 April 2018
Available online 17 April 2018

by organic sensitizers. A simplified version of the sensitized luminescence process comprises the following steps: i) the transition from the ground singlet state (S_0) to excited singlet states (S_n^*) of the complex molecule which involves the organic ligands, ii) the succeeding intersystem crossing (ISC) to one of its lower energy triplet states iii) the energy transfer to the emissive states of the Ln^{3+} ions and finally iv) the Ln^{3+} emission. The energy and features of the emissive states of the Ln^{3+} ions are well known and their energies are little affected by the organic ligands so it becomes of high importance the knowledge of the energy of the excited (either singlets and triplets) states of the organic chromophores, which is performed by spectroscopic studies of the isostructural Gd^{3+} complexes. The energy of the excited states of the Gd^{3+} ions is much higher than the energies of the excited states of the antennas and the ligand to metal energy transfer doesn't occur. Thus the luminescence of the Gd^{3+} complexes is due to the ligand centered fluorescence and phosphorescence which gives the energy of the excited singlet and triplet states of the antennas [13,16–22].

The ligand 1,10-phenanthroline (phen) is a "classic" and very suitable molecule for the synthesis of luminescent Eu^{3+} complexes for the following reasons: i) it shows a strong absorbance in the UV region that leads to a high population of its low-lying singlet states whose energy can be transferred to its triplet states; ii) the energy of the triplet states of the molecule are sufficiently above the lower lying emissive states of the Eu^{3+} (the $^5D_{0,1,2}$); and iii) the rigid structure imposed by the central ring and the direct Eu^{3+}–N bond lead to an efficient energy transfer between the excited states of the ligand and the emissive states of the Eu^{3+}. In particular, the complex $[Eu_2(phen)_2(bz)_6]$ was prepared and studied by Hui-Juan et al., they found the largest intrinsic luminescence quantum yield for Eu^{3+} in this complex compared with a series of Eu^{3+}-complexes [23]. All these interesting features apply for many phenanthroline derivatives and several works have been devoted to study and compare the phenanthroline and its derivatives [16–22]. It has been proved that the addition of substituents to an antenna chromophore leads to a change in the energy of its excited states which results in a change (and a tune, therefore) of the emissive properties of the complex [20,24–26]. Our contribution will deal with the changes in the structure and properties of the complex formed by the 4,7-biphenyl-1,10-phenanthroline compared to that formed by the 1,10-phenanthroline (bphen).

Because of the neutral character of the 4,7-biphenyl-1,10-phenanthroline ligand, it requires the concurrence of other anions in the complex formation to balance the + 3 charge of the Eu^{3+} ions. Our choice has been the benzoate (bz, the conjugate base of the benzoic acid), a simple and low-cost anionic ligand that shows strong absorbance in the UV region and very high quantum yields in the emissive processes [13].

Therefore, we have synthesized the complexes $[Eu_2(bphen)_2(bz)_6]$ (**1**) and $[Gd_2(bphen)_2(bz)_6]$ (**2**), and herein we show their crystal structure, thermal analyses and spectroscopic characterization. Finally, the performance for Si solar cells in the UV–VIS region was analysed via EQE measurements.

2. Experimental

2.1. Materials

Europium(III) oxide (99.99%), gadolinium(III) oxide (99.99%) 4,7-biphenyl-1,10-phenanthroline (bphen, 97%), phenanthroline (phen, 99%), analytic grade 1 M HCl solution, benzoic acid (Hbz, 99.99%), NaOH (99%) and spectroscopic grade CH_2Cl_2 were purchased from commercial sources and used as received. Poly(methylmethacrylate), PMMA, average Mw 996,000 was purchased from Aldrich (ref. 182265). Europium chloride, stock solution (0.2 M), was prepared by suspending 3.52 g of anhydrous europium oxide in 60 ml of 1 M HCl and digesting on a steam bath until completely dissolved. Then the solution was made up to a volume of 100 ml and kept in the refrigerator at 4 °C. Similarly, a stock solution of $GdCl_3$ (0.2 M) was also prepared.

2.2. Synthetic procedures

2.2.1. Synthesis of $[Eu_2(bphen)_2(bz)_6]$ (1) and $[Gd_2(bphen)_2(bz)_6]$ (2)

4,7-biphenyl-1,10-phenanthroline (100 mg, 0.301 mmol) was dissolved in 10 ml of ethanol, mixed with 1.5 ml of the $EuCl_3$ stock solution (0.3 mmol) and the mixture was heated at 60 °C under stirring in a round flask. In a separated beaker, benzoic acid (110.17 mg, 0.903 mmol) in ethanol (10 ml, 90%) was neutralized with an aqueous solution of NaOH 2 M (0.45 ml) and added under stirring to the previously prepared hot solution, a small amount of a white precipitate was formed. Then the mixture was refluxed for 3 h. After that time, a white product was obtained that was filtered, washed with water and dried in an oven at 80 °C overnight (yield 0.2019 g, 80%). IR (KBr) main bands: 3060-3030 (s, C–H aromatic), 1605(m, ν_{as}C=O) 1564, 1535 (m, C=C, C=N, aromatic), 1413 (s, ν_sC=O), 718 (s, mono-substituted benzene). Elemental analysis calculated (%) for $C_{90}H_{62}N_4Eu_2O_{12}$: C, 64.23; H, 3.69; N, 3.31. Found: C, 63.93; H, 3.75; N, 3.30. Formula weight: 1695.36 g mol^{-1}. Single crystals were obtained by diffusion of diethylether vapour into a chloroform solution of $[Eu_2(bphen)_2(bz)_6]$.

$[Gd_2(bphen)_2(bz)_6]$ was prepared in a similar way by using the appropriate amount of $GdCl_3$ solution instead of the $EuCl_3$ solution. IR (KBr) main bands: 3060-3030 (s, C–H aromatic), 1609(m, ν_{as}C=O) 1570, 1527 (m, C=C, C=N, aromatic), 1409 (s, ν_sC=O), 722 (s, mono-substituted benzene). Elemental analysis calculated (%) for $C_{90}H_{62}N_4Gd_2O_{12}$: C, 63.36; H, 3.66; N, 3.28. Found: C, 63.96; H, 3.67; N, 3.15. Formula weight: 1705.94 g mol^{-1}.

2.2.2. Synthesis of $[Eu_2(phen)_2(bz)_6]$

The compound was prepared following the same procedure using phenanthroline instead of 4,7-biphenyl-1,10-phenanthroline. This compound was synthesized for comparison purposes. (yield 0.1495 g, 72%). IR (KBr) main bands: 3060-3030 (s, C–H aromatic), 1611(m, ν_{as}C=O) 1568, 1532 (m, C=C, C=N, aromatic), 1423, 1408 (s, ν_sC=O), 720 (s, mono-substituted benzene). Elemental analysis calculated for $C_{66}H_{46}N_4Eu_2O_{12}$: C, 56.98; H, 3.33; N, 4.03. Found: C, 57.02; H, 3.34; N, 3.94. Formula weight: 1390.95 g mol^{-1} [14,23,25].

2.2.3. Preparation of the polymeric luminescent films

Samples containing 3.5 and 7.0 mg of $[Eu_2(bphen)_2(bz)_6]$ complex were dissolved in 7 ml of CH_2Cl_2 in a refrigerated ultrasonic bath, then, 70 mg of PMMA were added and the mixture stirred until complete solution of the polymer, obtaining samples with relative weight concentration of the active species of 5% and 10.0% respect to the PMMA. Spin-coating method (800 rpm for 7 s) was used to prepare the films on commercial PV glass substrates (20 × 20 mm, Pilkington). Once the solvent is evaporated the film contains a solid solution of the active species, $[Eu_2(bphen)_2(bz)_6]$, which keeps its composition and structure in PMMA.

2.3. Characterization

Elemental analyses (C, H and N) were performed on an EA 1108 CHNS-O microanalytical analyzer. IR spectra (400–4000 cm^{-1}) were recorded on a Thermo Nicollet avatar 360 FT-IR spectrometer with the sample prepared as KBr disks.

Simultaneous TG-DTA measurements were performed to $[Eu_2(bphen)_2(bz)_6]$ on a Perkin-Elmer differential thermal analyzer. Experiments were carried out in static air with a heating rate of 5 °C/min, in a temperature range of 25–875 °C. The sample mass was 3.25 mg.

UV–VIS spectra in dichloromethane (CH_2Cl_2) solution were performed for the benzoic acid, the bphen and phen ligands and the $[Eu_2(phen)_2(bz)_6]$ and $[Eu_2(bphen)_2(bz)_6]$ complexes in a concentration range of 1 × 10^{-6} M to 5 × 10^{-6} M, from 200 nm to 800 nm in a

Varian Cary 50 Bio UV–visible spectrophotometer at 25 °C. The phenanthroline ligand and derivative complex were included for comparison purposes.

Emission and excitation spectra were obtained by exciting the samples with light from a 300 W Xe arc lamp passed through a 0.25 m double-grating monochromator and detecting with a 0.25 m monochromator with a R928 photomultiplier. Low temperature emission spectra were acquired by using a He cycling cryogenerator.

Luminescence lifetimes were obtained by recording the emission decays after pulsed excitation at 355 nm by the 3rd harmonic of a YAG:Nd laser. The signal was detected by using a PMT together with a digital storage oscilloscope controlled by a personal computer. The time resolution of this setup was 20 ns.

The external quantum efficiency (EQE) measurements in the 280–1200 nm range have been acquired using a 100 W Xe arc lamp, double monochromator and a digital lock-in amplifier, integrated in the SPECLAB commercial setup at Fraunhofer ISE Laboratory and Servicentre (Gelsenkirchen, Germany). The different DS layers (deposited on glass) were directly placed on top of a p-type mc-Si solar cell (non-textured and with a SiN_x antireflecting coating optimized at 600 nm and encapsulated) to measure the improvements in EQE. The homogeneity of the DS layer for the different samples was also checked.

2.4. Crystallography

2.4.1. X-ray data collection and structure refinement

X-ray diffraction data on a single crystal of **1** was collected with a Rigaku SuperNOVA diffractometer with microfocus X-ray using Mo Kα radiation (λ = 0.71073 Å). CrysAlisPro software was used to collect, index, scale and apply numerical absorption correction based on gaussian integration over a multifaceted crystal model and empirical absorption correction using spherical harmonics, implemented in SCALE3 ABSPACK scaling algorithm into CrysAlisPro [27]. The structure was solved applying the novel dual-space algorithm implemented in SHELXT program [28]. Fourier recycling and least-squares refinement were used for the model completion with SHELXL-2014 [29]. All non-hydrogen atoms have been refined anisotropically, and all hydrogen atoms have been placed in geometrically suitable positions and refined riding with isotropic thermal parameter related to the equivalent isotropic thermal parameter of the parent atom. The geometrical analysis of interactions in the structure was performed with the Olex2 program [30]. The hydrogen atoms were geometrically positioned with C-H = 0.93 Å and Uiso(H) = 1.2 Ueq(C). Crystal data, collection procedures and refinement results are summarized in Table 1.

X-ray powder diffraction patterns on polycrystalline samples of $[Eu_2(bphen)_2(bz)_6]$ and $[Gd_2(bphen)_2(bz)_6]$ were collected with a PANanalytical X'pert X-ray diffractometer (Cu K_α radiation = 1.54184 Å) at room temperature (Fig. S2).

3. Result and discussion

3.1. Synthesis

The synthetic procedure provides a white crystalline material for all the compounds in high yields. However crystals suitable for single crystal X-ray diffraction had to be obtained by vapour-liquid diffusion and by this procedure very small single-crystal were obtained only for compound **1**. Nevertheless, these single-crystals were of enough quality to solve the structure of the compound. The polycrystalline material of **1** and **2** was of good quality for the thermogravimetric, X-ray powder diffraction and spectroscopic experiments. Moreover it had good solubility in CH_2Cl_2 for the preparation of the doped polymeric films.

3.2. Thermogravimetric analysis

The thermogravimetric analysis of $[Eu_2(bphen)_2(bz)_6]$ is shown in Fig. 1. Thermal decomposition of the complex starts about 300 °C with a mass loss of about 40% in a first step which corresponds to the decomposition of the bphen ligand [31]. It continues with the degradation of the benzoic acid and ends up with the formation of Eu_2O_3 above 800 °C [32]. This study shows the thermal stability of the complex to verify its applicability in the production process of PV modules where the temperature remains below 200 °C. Therefore, the $[Eu_2(bphen)_2(bz)_6]$ PMMA layer can be placed in any step of the module assembly of crystalline silicon solar cells, as the whole standard assembly process is performed at temperatures below 200 °C [33].

Table 1
Crystallographic data for compound $[Eu_2(bphen)_2(bz)_6]$.

Compound	$[Eu_2(bphen)_2(bz)_6]$
Empirical formula	$C_{90}H_{62}N_4O_{12}Eu_2$
Formula weight (g mol^{-1})	1695.36
T (K)	150 (1)
Crystal system	Triclinic
Space group	P − 1
a (Å)	11.6902 (6)
b (Å)	12.4766 (6)
c (Å)	14.2903 (7)
α (°)	102.448 (4)
β (°)	103.729 (4)
γ (°)	111.387 (5)
V (Å^3)	1777.07 (17)
Z	2
D_{calc} (g cm^{-3})	1.584
λ (Mo Kα) (Å)	0.71073
F(000)	852
Crystal dimensions (mm)	0.077 × 0.070 × 0.042
2θ range for data collection (°)	3.11–56.47
Limiting indices	− 14 ≤ h ≤ 15 − 16 ≤ k ≤ 16 − 18 ≤ l ≤ 18
Reflections (collected/unique, (Rint))	12788/7768/0.0289
Data/restraints/parameters	7768/0/487
R_1[a], wR_2 [$F^2 > 2\sigma(F^2)$][b]	0.0333/0.0856
Goodness-of-fit on F^2	1.072
Largest diff. peak and hole (e Å^{-3})	1.93/− 0.67
CCDC number	1494543

[a] $R_1 = \Sigma||F_0|-|F_c||/\Sigma|F_c|$.
[b] $wR_2 = (\Sigma[w(F_0^2-F_c^2)^2]/\Sigma[w(F_0^2)^2)^{1/2}$.

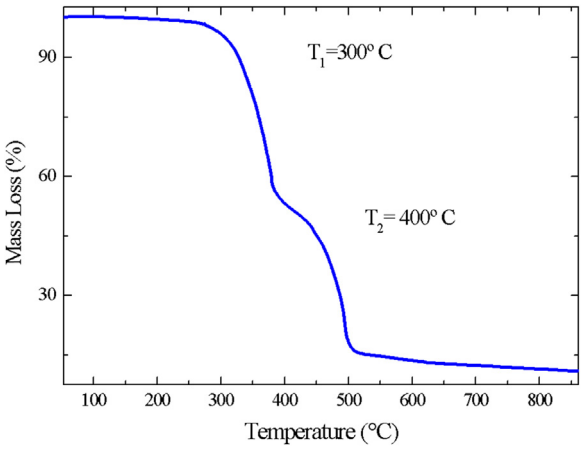

Fig. 1. Thermogravimetric plot for $[Eu_2(bphen)_2(bz)_6]$.

3.3. Description of the structure

The structure of $[Eu_2(bphen)_2(bz)_6]$, determined by single-crystal X-ray diffraction, consist of centrosymmetric dinuclear molecules in which the Eu atoms are octa-coordinated in an environment that could be roughly described as bicaped pentagonal-bipyramidal (Fig. 2). Three carboxylate-oxygens (O1B, O2B and $O1C^i$) and two bphen-nitrogen

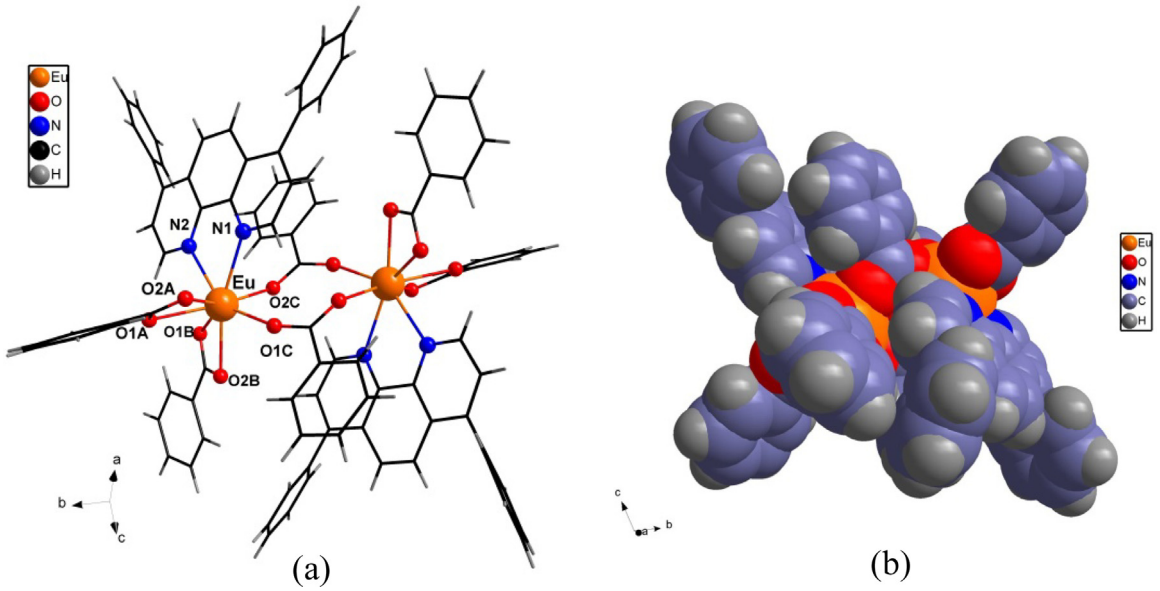

Fig. 2. (a) Molecular structure of $[Eu_2(bphen)_2(bz)_6]$. (b) Space-filling view of the molecule showing the aromatic rings on the periphery of the molecule enhancing its solubility in organic solvents.

Table 2
Selected distances for compound $[Eu_2(bphen)_2(bz)_6]$ and $[Eu_2(phen)_2(bz)_6]$ [34].

$[Eu_2(bphen)_2(bz)_6]$		$[Eu_2(phen)_2(bz)_6]$	
Atoms	[Å]	Atoms	[Å]
Eu1—O2A	2.4398(2)	Eu1—O2	2.4933(11)
Eu1—O1A	2.4494(2)	Eu1—O1	2.4974(11)
Eu1—O1B	2.3988(1)	Eu1—O6^{ii}	2.3818(10)
Eu1—O2B	2.4376(1)	Eu1—O4	2.4571(11)
Eu1—O1C	2.3138(1)	Eu1—O3^{ii}	2.3669(9)
Eu1—O2C^{i}	2.3239(2)	Eu1—O5	2.3667(9)
Eu1—N1	2.5728(1)	Eu1—N1	2.5636(11)
Eu1—N2	2.5817(1)	Eu1—N2	2.6134(11)
Eu1—Eu1^{i}	5.5441(3)	Eu1—Eu1^{ii}	3.9604(1)
(i) 1-x, 2-y, 1-z.		(ii) 2-x, -y, 1-z.	

atoms (N1 and N2) fill the pentagonal equatorial plane and three carboxylate-oxygens (O1A, O2A and O2C) fill the axial positions (symmetry code i = 1-*x*; 2-*y*; 1-*z*). The compound lacks of coordination water molecules which is a very interesting feature for its luminescent properties. In the dinuclear complex the two bphen and four benzoate molecules work as terminal ligands with a η^2-coordination mode for this latter ligand: atoms O1A, O2A, O1B, O2B and symmetry related O1A^{i}, O2A^{i}, O1B^{i}, O2B^{i}. Whereas the other two benzoate molecules bridge the Eu^{3+} ions with the two carboxylate groups adopting a *syn-syn* bridging mode (μ:η^1-η^1), atoms: O1C, O2C, O1C^{i}, O2C^{i}. The Eu—O and Eu—N distances span in their normal ranges from 2.3138(1) Å to 2.4494(1) Å and 2.5728(1) Å to 2.5817(1) Å, respectively. The structure and the Eu—O and Eu—N distances are very similar to those found in $[Eu_2(phen)_2(bz)_6]$ (Table 2) with the exception that in that case four benzoate molecules acted as bridging ligands (and only two in the case of $[Eu_2(bphen)_2(bz)_6]$). This resulting in a rather long Eu···Eu distance in **1**, 5.5441(1) Å, compared to that found in $[Eu_2(bphen)_2(bz)_6]$, 3.9604(1) Å [34,35], Fig. S1 (c). In the formation of the luminescent films, the structure of the complex is maintained, so the Eu^{3+}-Eu^{3+} distance is that of the molecular structure.

The two phenylene rings of the bphen ligands appear twisted respect to the plane of the phenanthroline skeleton and another remarkable feature of the compound is the almost parallel orientation of the bridging benzoate ligand respect to the phenanthroline central aromatic ring, see Fig. S1 (a) (ESI). Molecular packing consist on weak hydrogen bonds with inter and intra molecular bonds and very weak π-π and π-Centroid interactions (Table S1). The molecular structure of the compound favours its solubility in organic solvents such as CH_2Cl_2.

The simulated powder diffraction pattern of the crystalline structure of single-crystals of **1** completely matches with the powder diffraction pattern of the polycrystalline material of **1**. So single-crystals and polycrystalline material have the same structure, Fig. S2. In the same way, powder diffraction patterns of $[Eu_2(bphen)_2(bz)_6]$ and $[Gd_2(bphen)_2(bz)_6]$ are equivalent which means unequivocally that both compounds display the same structure, Fig. S2.

3.4. Solution studies. UV–VIS spectra

UV–VIS absorption spectra of $[Eu_2(phen)_2(bz)_6]$ and $[Eu_2(bphen)_2(bz)_6]$ complexes in CH_2Cl_2 are presented in Fig. 3. The spectrum of $[Eu_2(bphen)_2(bz)_6]$ shows one intense absorption with a maximum at 290 nm with a corresponding molar absorption coefficient

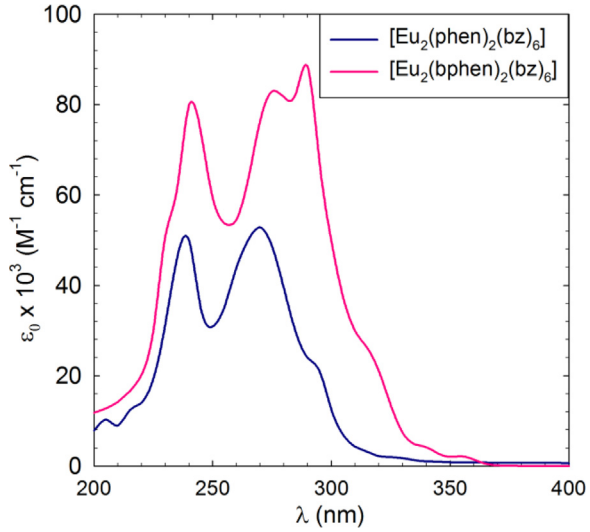

Fig. 3. Absorption spectra of $[Eu_2(phen)_2(bz)_6]$ and $[Eu_2(bphen)_2(bz)_6]$ in CH_2Cl_2 at 2.5×10^{-6} M.

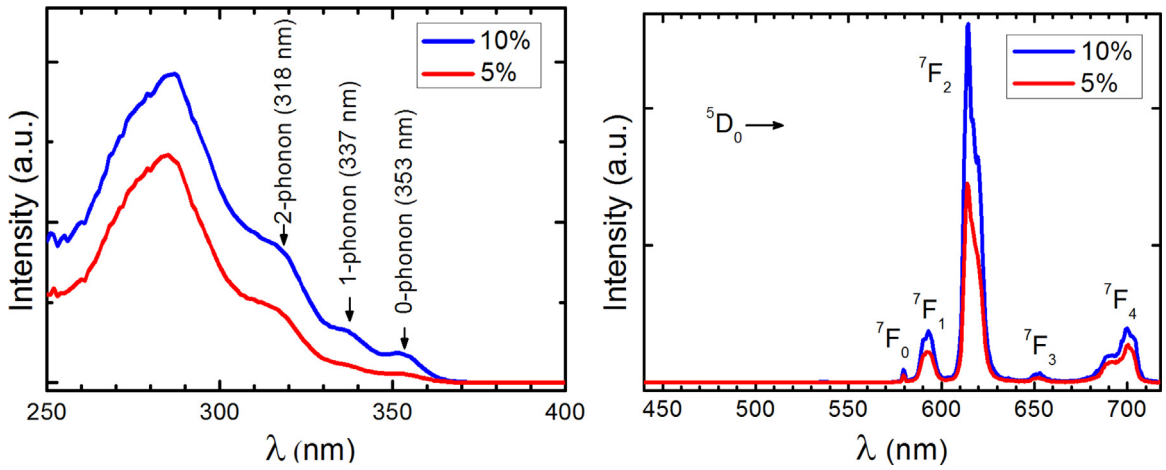

Fig. 4. Antenna excitation (left) and corresponding Eu^{3+} emission (right) spectra of $[Eu_2(bphen)_2(bz)_6]$ at 5% (red line) and 10% (blue line) in PMMA.

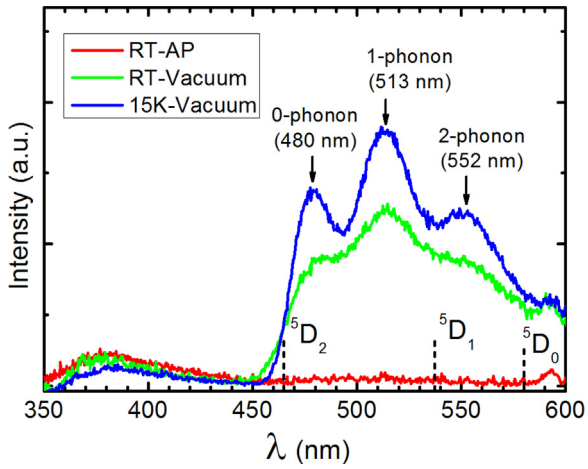

Fig. 5. Photoluminescence (fluorescence and phosphorescence) spectra for the film containing the $[Gd_2(bphen)_2(bz)_6]$ complex at 10% in PMMA under excitation at 280 nm, at room temperature (RT-AP) and atmospheric pressure (red line), RT and vacuum conditions (green line) and at 15 K and vacuum (blue line). Dashed vertical lines point the direct excitation energies of Eu^{3+} ions from the fundamental energy level.

of 88400 L mol^{-1} cm^{-1}. Other lower absorption maxima are observed at 242 and 276 nm and some shoulders are found at 316, 340 and 355 nm. Compared to $[Eu_2(phen)_2(bz)_6]$, $[Eu_2(bphen)_2(bz)_6]$ shows a considerable increase in the absorption coefficient that is almost doubled at the maxima. Also, the absorbance is higher than that of the reference complex in all analysed wavelengths. This is somewhat expected since the bphen ligand itself exhibits higher absorption compared to phen (Fig S3, ESI). This increase in the absorption is usually correlated with an increase in the emission so, for instance, this points to an enhancement of the properties of $[Eu_2(bphen)_2(bz)_6]$ compared to the reference complex, $[Eu_2(phen)_2(bz)_6]$. Maxima and shoulders values observed in the spectrum give the energy of the allowed S_0— > S_n^* transitions. With this information, the energy of the excited singlet states can be inferred.

3.5. Photophysical properties (PMMA films)

The excitation and emission spectra of $[Eu_2(bphen)_2(bz)_6]$ at 5% and 10% in PMMA films are shown in Fig. 4. The excitation spectra of the $^5D_0 \rightarrow {}^7F_2$ emission of Eu^{3+} ions at 614 nm display a broad band between 250 and 350 nm with a maximum at 280 nm. This result shows an efficient UV sensitization of these ions by means of ligand to metal energy transfer processes, with the ligand acting as antenna. Its maximum value is close to the maximum observed in the UV–VIS absorption spectrum and presents a similar behaviour. The excitation spectra show a discrete vibrational structure that enables the detection of vibronic transitions with creation of 0, 1 or 2 phonons, as indicated in Fig. 4 (left). This vibrational structure is also similar to the one observed in the absorption spectra of this complex shown in Fig. 3. The observed peak at 280 nm results from the overlap of different multiphonon side peaks, which are not well resolved and therefore appears as a multiphonon band.

The emission spectra, under 280 nm excitation, reveals the characteristic emission peaks of Eu^{3+} ions corresponding to the transitions $^5D_0 \rightarrow {}^7F_{0-4}$, being the emission at 614 nm ($^5D_0 \rightarrow {}^7F_2$) the most intense transition and responsible for the brilliant red emission of this complex. Only the emissions from the $^5D_0$ level are observed due to fast non-radiative decays from upper levels to this emitting level. These spectra present large inhomogeneous broadening, not being possible to resolve the Stark components of the different emission peaks. This broadening is caused by distortion of the local environment of the Eu^{3+} ions. The intensity of the excitation and emission spectra obtained for the active film is increased by a factor of almost 2 when the concentration of the luminescent complex is doubled, as seen in Fig. 4. These spectra show only emission from Eu^{3+} ions, without any appreciable contribution from the triplet state, indicating that the energy transfer from the antenna to the lanthanides is highly efficient.

A study of the luminescent properties (fluorescence and phosphorescence) of $[Gd_2(bphen)_2(bz)_6]$ was carried out, at room and low temperature, to determine the triplet and singlet state energies of the compound, Fig. 5. The emitting levels of the Gd^{3+} ions are far above the triplet levels of the ligands and therefore metal-centered emissions do not take place in these complexes. Moreover, its paramagnetic character is known to enhance the intersystem crossing and furthermore the presence of the Gd^{3+} ion reduces the decay time of the triplet states. So, all these conditions make the Gd^{3+} derivatives good candidates to study the energy of the singlet and triplet states of the lanthanide luminescent complexes [13,15,21,22,36].

The photoluminescence spectra obtained for the film containing the $[Gd_2(bphen)_2(bz)_6]$ complex at 10% in PMMA, under different conditions, are shown in Fig. 5. These spectra have two main emissions, a relatively weak UV-Violet emission at 380 nm coming from the excited singlet state, together with a broad whitish emission arising from the decay of the triplet state of these organic molecules. The whitish VIS emission comprises three well resolved vibronic components at 480, 513 and 552 nm (corresponding to transitions with creation of 0, 1 or 2 phonons, respectively) and a multiphonon tail at long-wavelengths.

It would be noticed that the emission spectra obtained with the

layer in air, at atmospheric pressure (RT-AP, Fig. 5), only shows the singlet emission. Whereas the spectra obtained with the sample in vacuum present a relatively intense emission coming from the triplet state. This behaviour is due to the quenching of the triplet emission by the dioxygen molecules when the films are in contact with air. Moreover, this response results to be reversible, what turns this complex into a good candidate for high resolution oxygen sensing [15,21]. On the other hand, the compound shows moderate increase of the emission when the temperature is lowered to 15 K, indicating a low thermal quenching of the triplet states at room temperature [11,37,38].

The luminescence quantum yield Φ is a parameter used to evaluate the efficiency of the emission process in luminescent materials, defined as the ratio of number of emitted photons to the number of absorbed photons per time unit. The luminescence quantum yield of lanthanide complexes is given by [13,15]:

$$\Phi = \Phi_{ET}\Phi_{Ln} \quad (1)$$

where Φ_{ET} is the efficiency of the energy transfer from the ligand to the lanthanide and Φ_{Ln} is the intrinsic luminescence quantum yield of the lanthanide, which can be obtained by

$$\Phi_{Ln} = \frac{A_{rad}}{A_{rad} + A_{nrad}} = \frac{\tau_{exp}}{\tau_{rad}} \quad (2)$$

where A_{rad} and A_{nrad} are the radiative and non-radiative decay probabilities and τ_{exp} and τ_{rad} are the experimental and radiative lifetimes, respectively.

In order to check the antenna-Eu^{3+} energy transfer efficiency we have measured the photoluminescence emission of $[Eu_2(bphen)_2(bz)_6]$ at 10% of PMMA at room and low temperature in vacuum and the results are shown in Fig. 6. These spectra show that the antenna emission from the triplet state (observed when the sample is doped with Gd^{3+}) is completely quenched when doping with Eu^{3+} (Fig. 5). This behaviour indicates a high value for the antenna-Eu^{3+} energy transfer efficiency, Φ_{ET}, close to 1.

On the other hand, the emission from the $^5D_0$ level of Eu^{3+} usually presents high quantum efficiency, Φ_{Ln}, due to the large gap to the underlying level $^7F_6$, about 12000 cm^{-1}, which prevents non-radiative decays. In our case, as shown in Fig. 6, the PL intensity does not change appreciably when temperature is lowered from RT to 15 K, indicating the absence of thermal quenching by nonradiative decays.

Low nonradiative decay rates are confirmed by the analysis of the experimental lifetime results. An experimental lifetime of 0.96 ms was obtained for Eu^{3+} luminescence at room temperature, see inset in Fig. 6. The radiative lifetime of the Eu^{3+} emitting level $^5D_0$ is mainly determined by the ratio $^5D_0 \rightarrow {}^7F_2$ / $^5D_0 \rightarrow {}^7F_1$ of the most intense

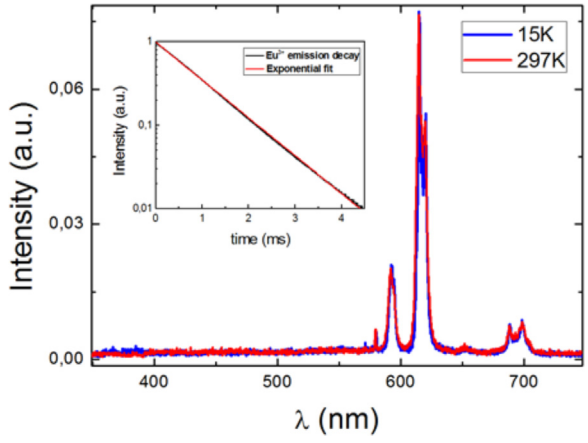

Fig. 6. Emission spectra for $[Eu_2(bphen)_2(bz)_6]$ at 10% of PMMA film under 280 nm excitation at room temperature (297 K) and low temperature (15 K) in vacuum condition. Inset shows the experimental lifetime of Eu^{3+} luminescence at RT.

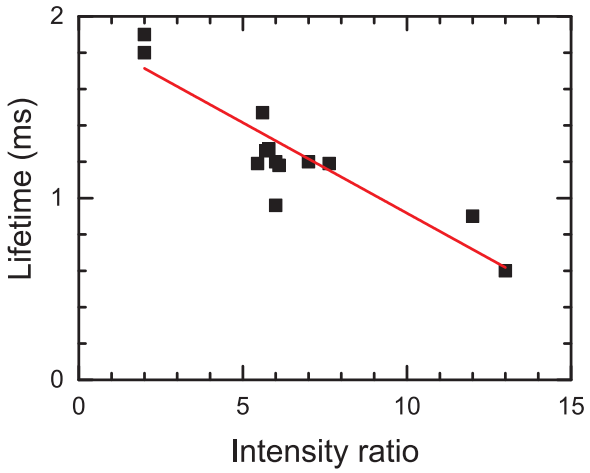

Fig. 7. Variation of the lifetime of the Eu^{3+} emitting level $^5D_0$ with the $^5D_0 \rightarrow {}^7F_2$ / $^5D_0 \rightarrow {}^7F_1$ intensity ratio for different Eu^{3+} complexes (data from this work and from Refs. [26] and [39]). Red line corresponds to linear fit.

emissions. The transition $^5D_0 \rightarrow {}^7F_2$ is electric dipolar and hypersensitive to the local environment of the Eu^{3+} ions. Meanwhile, the transition $^5D_0 \rightarrow {}^7F_1$ is magnetic dipolar and presents low dependence on the local environment. The above ratio is indicative of how far is the local Eu^{3+} environment to be centrosymmetric. Following these considerations, for low nonradiative rates, a correlation of the experimental lifetime and the intensity ratio is expected, i.e., a decrease of the lifetime would be found when the intensity ratio increases. Accordingly, longer lifetimes of ~ 1.8–1.9 ms were obtained at 77 and 295 K for [Eu(phen)(3,5-DNBenz)$_3$], (3,5-DNBenz = 3,5-dinitrobenzoate anion) indicating low nonradiative rates, which is associated with a low intensity ratio of about 2 [26]. Meanwhile, we obtained a experimental lifetime of 0.96 ms with a higher intensity ratio of 6.0, from spectra in Fig. 6, which is well correlated with results for other Eu^{3+} complexes, as ternary methoxybenzoates [26]. Moreover, our results are comparable with the values obtained for the complex $[Eu_2(phen)_2(bz)_6]$ of 1.26 ms and 5.7 for the lifetime and intensity ratio, respectively [39]. Additionally, lower lifetimes of ~ 0.6–0.9 ms have been obtained with high intensity ratios of ~ 12–13 for β-diketonates [26]. These results, shown in Fig. 7, corroborate that nonradiative processes are not significant in our samples.

In the literature, the intrinsic luminescence quantum yield Φ_{Ln} for the Eu^{3+} ions is frequently calculated by using the Eq. (2) with the radiative lifetime obtained from the following expression [40–43]:

$$\tau_{rad} = \frac{1}{n^3 A_{MD,0}} \frac{I_{MD}}{I_{tot}} \quad (3)$$

where $A_{MD,0} = 14.65\ s^{-1}$ is the spontaneous emission probability for the $^5D_0 \rightarrow {}^7F_1$ transition in vacuo, (I_{MD}/I_{tot}) is the ratio between the integrated intensity of the $^5D_0 \rightarrow {}^7F_1$ transition and the total integrated emission intensity $^5D_0 \rightarrow {}^7F_J$ (J = 0–6) and n is the refractive index of the medium related with Lorentz local field correction.

In this line, Eu^{3+} radiative lifetimes of about 2 ms have been reported for similar complexes using Eq. (3) and assuming a general value for the refractive index of 1.5 [41,42]. This estimation of the radiative lifetime would lead to a value for the efficiency Φ_{Ln} of about 0.5 in our samples. Nevertheless, it is important to stress that a consistent determination of the refractive index is necessary in order to obtain reliable results from Eq. (3), due to the strong dependence of the radiative lifetime on this parameter.

Finally, a high luminescence quantum yield Φ is expected from Eq. (1) in our Eu^{3+} complex, which would be at least 0.5, taking into account the estimated values for the efficiencies of the energy transfer to the Eu^{3+} ions, Φ_{ET}, and the luminescence of the Eu^{3+} ions, Φ_{Ln}. This

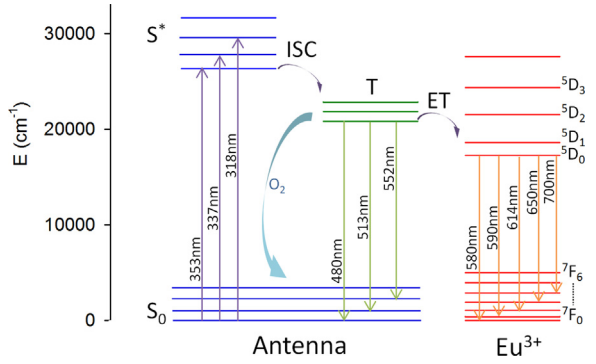

Fig. 8. Photophysical processes in $[Eu_2(bphen)_2(bz)_6]$ under UV excitation taking to Eu^{3+} red emission (antenna effect). The wavelengths determined from spectra in Figs. 3–5 are indicated.

result would not be far from the highest values we have found in literature, which are about 0.8 ± 0.1 for Eu^{3+} in different complexes such as $[EuL(tta)_3]$, with tta = 2-thenoyltrifluoroacetylacetonate and L = 4,7-dicarbazol-9-yl-[1,10]-phenanthroline ([24] and references therein).

3.6. Energy level diagram and sensitized luminescence mechanism

Fig. 8 shows the energy level diagram of the singlet and triplet states of the antenna and those excited states of the Eu^{3+}, which are directly related with the quantum yield of the overall luminescence process. The vibrational levels into the singlet and triplet states of the antenna are also displayed [44]. The diagram shows the excitation of the antenna from the ground S_0 to the excited S^* singlet state, followed by ISC to the triplet T state and energy transfer to Eu^{3+} ions. The UV–VIS absorption, excitation and emission spectra (Figs. 3–5) allowed us to calculate the energy of singlet and triplet states of the antenna, which display a separation larger than 6000 cm^{-1}. This satisfies the criterion for an efficient ISC according to different authors [45].

The transitions from the triplet state were determined from the emission spectra in Fig. 5. This emission presents a large overlap with the excitation of the $^5D_{0,1,2}$ levels of Eu^{3+} from the ground level $^7F_0$. This can be verified from Fig. 5 where the wavelengths of these transitions have been indicated. Therefore, the $^5D_{0,1,2}$ levels of Eu^{3+} would be the main acceptors of energy transfer from the triplet states of $[Eu_2(bphen)_2(bz)_6]$ complex. Some authors claim that efficient ET transfer occurs when the energy difference between the triplet state of the antenna and the Ln emissive levels is of approximately ~ 2000–3500 cm^{-1} (others extend this range from 1000 to 5000 cm^{-1}) [15,44]. This condition is also satisfy by $[Eu_2(bphen)_2(bz)_6]$.

Finally, the excited Eu^{3+} ions undergo to the $^7F_0$ level involving $^5D_0 \rightarrow {}^7F_J$ radiative transitions, see Fig. 4. On the other hand, the emitting $^5D_0$ level of Eu^{3+} is about 3590 cm^{-1} below the triplet state of the antenna, see Fig. 8. Therefore, appreciable back-transfer from Eu^{3+} to antenna would not be expected.

3.7. External quantum efficiency

The influence of the down-shifting film on a reference cell is calculated by means of an external quantum efficiency measurement (EQE). The EQE of the reference solar cell covered with a bare glass substrate, and the reference solar cell covered with the same type of glass substrate but coated with the luminescent film at different concentrations are displayed in Fig. 9. Consequently, a thin film of air is located between the glass substrate and the reference cell producing a discontinuity in refractive indexes and, consequently, lowering the overall EQE values. This configuration was used to obtain reproducibility of the results, to avoid any damage to the reference solar cell and contamination using any other procedure involving chemicals to match the refractive indexes. Measurements were taken with the downshifting layer on the front side of the glass. EQE measured at the UV spectral region diminish a 22% when the reference solar cell is only covered with the bare glass, due to the absorption of UV photons by the glass substrate and the discontinuity in refractive indexes. An enhancement of the conversion efficiency in the UV range has been recorded for 5% $[Eu_2(bphen)_2(bz)_6]$ and 10% $[Eu_2(bphen)_2(bz)_6]$ films with maximum energy conversion at 290–300 nm. This increase in efficiency at the UV spectral region correlates with the absorption and excitation spectra analysed in Fig. 4. In comparison with the measurement only with the bare glass, where a near-zero EQE is detected in the 280–360 nm spectral range, significative EQE signals are detected for the reference solar cells with the luminescent film deposited on glass and placed on top, reaching a 4.6% peak for the 10% $[Eu_2(bphen)_2(bz)_6]$ PMMA film and a 3.5% peak for the 5% $[Eu_2(bphen)_2(bz)_6]$ PMMA film. The EQE spectra measured in the 280–1200 nm spectral range (Fig. 9b) show the transparency of the active layer in the visible spectrum, at these concentrations. Of course, the EQE is expected to be substantially improved by increasing the concentration of $[Eu_2(bphen)_2(bz)_6]$ and avoiding the air gap between the glass and the reference solar cell via encapsulation processes with EVA or any other transparent polymer matching the refraction index between both media.

4. Conclusions

The complexes $[Eu_2(bphen)_2(bz)_6]$ (**1**) and $[Gd_2(bphen)_2(bz)_6]$ (**2**) have been successfully obtained by direct synthesis and characterized by FT-IR, TGA, X-ray diffraction and elemental analyses. The match of the X-ray powder diffraction patterns of both compounds shows their isostructural character and the X-ray analysis of single-crystals of **1** reveals their molecular structure, in which the organic ligands wrap the Ln^{3+} ions avoiding coordination water molecules and giving good solubility in organic solvents such as CH_2Cl_2. PMMA films containing this luminescent complexes have been prepared by simple spin-coating on glass substrates to cover a reference solar cell, showing enough thermal stability to be incorporated in the processing of PV cells and modules in any step of the production process. The bphen and bz ligands absorb UV photons and efficiently transfer energy to the Eu^{3+} ions, which are promoted to the $^5D_{0-2}$ excited states and subsequently decay from the $^5D_0$ to the $^7F_{0-6}$ states, by emitting intense red radiation. The study of the energy levels of the singlet and triplet states of the organic chromophore has shown the existence of vibrational levels in the ground and excited singlet states of the antenna where the involvement of 0, 1 or 2 phonons has been detected. Initial results show that the downshifting of the UV photons increases the delivered power of PV cells in the region between 280 and 360 nm for PMMA films containing the luminescent compound, reaching a 4.6% increment of EQE at 297 nm. Finally, the PPMA films prepared with the $[Gd_2(bphen)_2(bz)_6]$ complex show high sensitivity to O_2 which may result in application as oxygen sensor.

Acknowledgements

This work has been supported by the Ministerio de Economía y Competitividad, Spain, Project ENE2013-41925 and Project MAT2016-75586-C4-4-P and co-supported by the European Social Fund.

Appendix A. Supplementary material

Crystallographic data for the structure reported in this contribution has been deposited within the Cambridge Crystallographic Data Centre as supplementary publication 1494543. Copies of the data can be obtained free of charge on application to the CCDC, Cambridge, U.K. ⟨http://www.ccdc.cam.ac.uk/⟩. Moreover, supplementary data associated with this article can be found in the online version at ⟨http://dx.

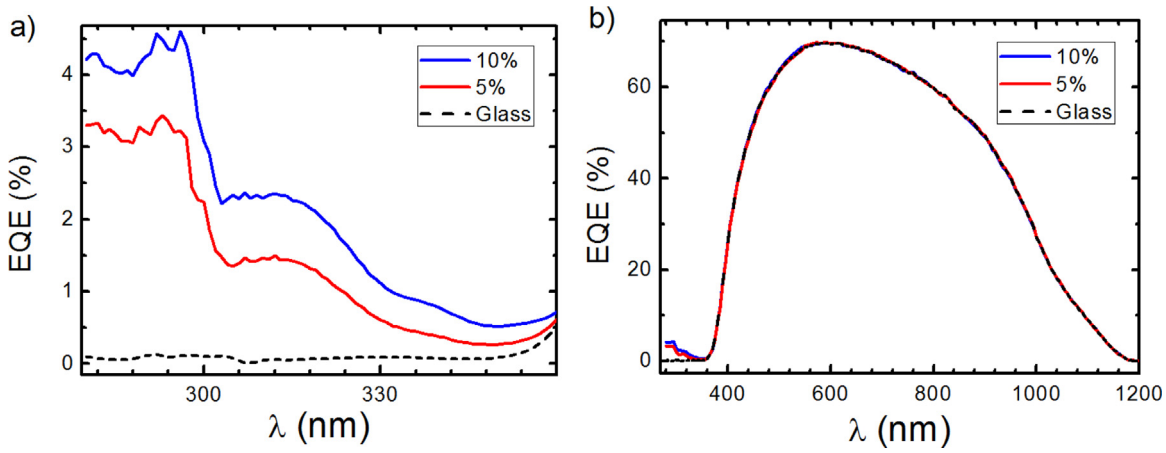

Fig. 9. EQE measurements in the UV range (a) and UV–VIS range (b), for the reference solar cell (RSC) covered with the clean glass (black dashed line) and with 5% $[Eu_2(bphen)_2(bz)_6]$ (red line) and 10% $[Eu_2(bphen)_2(bz)_6]$ (blue line) PMMA films on top.

doi.org/10.1016/1494543〉.

Appendix A. Supporting information

Supplementary data associated with this article can be found in the online version at https://doi.org/10.1016/j.jlumin.2018.04.038.

References

[1] IRENA (05/2017), 〈http://resourceirena.irena.org/gateway/dashboard/ 〉.
[2] Photovoltaics Report. Fraunhofer Institut for Solar Energy Systems. July, 〈https://www.ise.fraunhofer.de/de/downloads/pdf-files/aktuelles/photovoltaics-report-in-englischer-sprache.pdf〉, 2017.
[3] E. Klampaftis, B.S. Richards, Prog. Photovolt. Res. Appl. 19 (2011) 345–351.
[4] T. Trupke, M.A. Green, P. Würfel, J. Appl. Phys. 92 (2002) 1668–1674.
[5] A. Boccolini, J. Marques-Hueso, D. Chen, Y. Wang, B.S. Richards, Sol. Energy Mater. Sol. Cells 122 (2014) 8–14.
[6] W.-J. Ho, Y.-J. Deng, J.-J. Liu, S.-K. Feng, J.-C. Lin, Materials 10 (2017) 21.
[7] N. Chander, S.K. Sardana, P.K. Parashar, A.F. Khan, S. Chawla, V.K. Komarala, IEEE J. Photovolt. 5 (2015) 1373–1379.
[8] A. Le Donne, M. Acciarri, D. Narducci, S. Marchionna, S. Binetti, Prog. Photovolt. Res. Appl. 17 (2009) 519–525.
[9] K. Lunstroot, K. Driesen, P. Nockemann, L. Viau, P.H. Mutin, A. Vioux, K. Binnemans, Phys. Chem. Chem. Phys. 12 (2010) 1879–1885.
[10] T. Fix, A. Nonat, D. Imbert, S. Di Pietro, M. Mazzanti, A. Slaoui, L.J. Charbonnière, Prog. Photovolt. Res. Appl. 24 (2016) 1251–1260.
[11] S.M. Borisov, R. Fischer, R. Saf, I. Klimant, Adv. Funct. Mater. 24 (2014) 6548–6560.
[12] H.A. Hoppe, Angew. Chem. Int. Ed. Engl. 48 (2009) 3572–3582.
[13] K. Binnemans, Chem. Rev. 109 (2009) 4283–4374.
[14] T. Monzón-Hierro, J. Sanchiz, S. González-Pérez, B. González-Díaz, S. Holinski, D. Borchert, C. Hernández-Rodríguez, R. Guerrero-Lemus, Sol. Energy Mater. Sol. Cells 136 (2015) 187–192.
[15] K. Binnemans, Coord. Chem. Rev. 295 (2015) 1–45.
[16] H. Wu, Q.Y. Wu, C.Z. Wang, J.H. Lan, Z.R. Liu, Z.F. Chai, W.Q. Shi, Dalton Trans. 45 (2016) 8107–8117.
[17] M.M. Nolasco, P.M. Vaz, V.T. Freitas, P.P. Lima, P.S. André, R.A.S. Ferreira, P.D. Vaz, P. Ribeiro-Claro, L.D. Carlos, J. Mater. Chem. A 1 (2013) 7339.
[18] E. Moretti, A. Talon, L. Storaro, A. Le Donne, S. Binetti, A. Benedetti, S. Polizzi, J. Lumin. 146 (2014) 178–185.
[19] X.-N. Li, Z.-J. Wu, Z.-J. Si, Z. Liang, X.-J. Liu, H.-J. Zhang, Phys. Chem. Chem. Phys. 11 (2009) 9687.
[20] M.M. Nolasco, P.D. Vaz, L.D. Carlos, New J. Chem. 35 (2011) 2435.
[21] L. Armelao, S. Quici, F. Barigelletti, G. Accorsi, G. Bottaro, M. Cavazzini, E. Tondello, Coord. Chem. Rev. 254 (2010) 487–505.
[22] S.V. Eliseeva, J.C. Bunzli, Chem. Soc. Rev. 39 (2010) 189–227.
[23] H.-J. Sun, X.-T. Fu, H.-B. Chu, Y. Du, X.-M. Lin, X. Li, Y.-L. Zhao, J. Photochem. Photobiol. A Chem. 219 (2011) 243–249.
[24] G. Zucchi, V. Murugesan, D. Tondelier, D. Aldakov, T. Jeon, F. Yang, P. Thuery, M. Ephritikhine, B. Geffroy, Inorg. Chem. 50 (2011) 4851–4856.
[25] S.Y. Niu, G.-X. Jin, W.M. Bu, G.D. Yang, J.Q. Cao, B. Yang, Chin. J. Struct. Chem. 18 (1999) 245–248.
[26] V. Tsaryuk, V. Kudryashova, P. Gawryszewska, R. Szostak, A. Vologzhanina, K. Zhuravlev, Z. Klemenkova, J. Legendziewicz, V. Zolin, J. Photochem. Photobiol. A Chem. 239 (2012) 37–46.
[27] Rigaku Oxford Diffraction, CrysAlisPro Software System, Version 1.171.38 43 Rigaku Corporation, Oxford, UK, 2015.
[28] G.M. Sheldrick, Acta Cryst. A71 (2015) 3–8.
[29] G.M. Sheldrick, Acta Crystallogr. C Struct. Chem. 71 (2015) 3–8.
[30] O.V. Dolomanov, L.J. Bourhis, R.J. Gildea, J.A.K. Howard, H. Puschmann, J. Appl. Cryst. 42 (2009) 339–341.
[31] S. Liu, R. Ma, J. Cryst. Growth 169 (1996) 190–192.
[32] I.G. Fomina, Z.V. Dobrokhotova, V.O. Kazak, G.G. Aleksandrov, K.A. Lysenko, L.N. Puntus, V.I. Gerasimova, A.S. Bogomyakov, V.M. Novotortsev, I.L. Eremenko, Eur. J. Inorg. Chem. 2012 (2012) 3595–3610.
[33] L. Katsikas, M. Avramovic, B. Cortés, M. Milovanovic, M. Kalagasidis-Krusic, I. Popovic, J. Serbian Chem. Soc. 73 (2008) 915–921.
[34] P.H. Ooi, S.G. Teoh, C.S. Yeap, H.K. Fun, Acta Cryst. E66 (2010) m597–m598.
[35] S.Y. Niu, B. Yang, J.Q. Cao, G.D. Yang, W.M. Bu, Kao Teng Hsueh Hsiao Hua Heush Hsueh Pao/Chem. J. Chin. Univ. 18 (1997) 1917–1920.
[36] C. Xu, Mon. für Chem. Chem. Mon. 141 (2010) 631–635.
[37] S.M. Borisov, O.S. Wolfbeis, Anal. Chem. 78 (2006) 5094–5101.
[38] I. Bergman, Nature 218 (1968) (396–396).
[39] K.P. Zhuravlev, V.I. Tsaryuk, I.S. Pekareva, J. Sokolnicki, Z.S. Klemenkova, J. Photochem. Photobiol. A Chem. 219 (2011) 139–147.
[40] M.H.V. Werts, R.T.F. Jukes, J.W. Verhoeven, Phys. Chem. Chem. Phys. 4 (2002) 1542–1548.
[41] I.G. Fomina, A.B. Ilyukhin, Y.S. Zavorotny, V.I. Gerasimova, I.V. Taidakov, N.P. Datskevich, A.G. Vitukhnovskii, Z.V. Dobrokhotova, I.L. Eremenko, Polyhedron 129 (2017) 105–113.
[42] R. Devi, Priyanka, S. Chahar, S.P. Khatkar, V.B. Taxak, P. Boora, Inorg. Chim. Acta 471 (2018) 364–371.
[43] N.M. Shavaleev, S.V. Eliseeva, R. Scopelliti, J.C. Bunzli, Inorg. Chem. 54 (2015) 9166–9173.
[44] Y. Ma, Y. Wang, Coord. Chem. Rev. 254 (2010) 972–990.
[45] H.-F. Li, P.-F. Yan, P. Chen, Y. Wang, H. Xu, G.-M. Li, Dalton Trans. 41 (2012) 900–907.